AIAA JOURNAL
Vol. 43, No. 4, April 2005

Unsteady Calibration of Fast-Response Pressure Probes, Part 3: Air-Jet Experiments

Espen S. Johansen* and Othon K. Rediniotis†
Texas A&M University, College Station, Texas 77843-3141

A facility was developed that produces a known and repeatable oscillating air jet used to test the unsteady probe calibration techniques developed in Parts 1 and 2 (Johansen, E. S., and Rediniotis, O. K., "Unsteady Calibration of Fast-Response Pressure Probes, Part 1: Theoretical Studies," *AIAA Journal*, Vol. 43, No. 4, 2005, pp. 816–826; Johansen, E. S., and Rediniotis, O. K., "Unsteady Calibration of Fast-Response Pressure Probes, Part 2: Water-Tunnel Experiments," *AIAA Journal*, Vol. 43, No. 4, 2005, pp. 827–834) for fast-response, multihole pressure probes. Its characteristics in the steady and unsteady operation modes were studied. The facility can produce flow velocities up to Mach 0.3 with oscillation frequencies up to 1500 Hz and oscillation amplitudes of up to ±20%. A hemispherical-tip, fast-response five-hole probe was developed and tested in this facility. The unsteady flowfield was measured via hot-wire anemometry, to document the instantaneous unsteady flow velocity, and a specially designed fast-response static-pressure probe in order to measure the jet's instantaneous unsteady static pressure. From the collected data, verification of the instantaneous flow angle and velocity prediction procedures was undertaken. These techniques require the use of the steady and unsteady pressures coefficients of the probe. The steady coefficient of the probe was measured in the facility, whereas the unsteady coefficient was taken from unsteady potential flow theory. Excellent prediction capabilities are demonstrated for both the flow angles and the instantaneous velocity magnitude.

Nomenclature

B_β	=	yaw-angle pressure coefficient
Cp	=	pressure coefficient
Cp_S	=	steady pressure coefficient
Cp_{STEADY}	=	steady pressure coefficient
Cp_U	=	unsteady pressure coefficient
Cp_{UNSTEADY}	=	unsteady pressure coefficient
K	=	nondimensional acceleration
M	=	Mach number
p	=	pressure, Pa
p_s	=	static pressure, Pa
$p_{\text{s\_Exit}}$	=	static pressure at the nozzle exit of the facility, Pa
$p_{\text{s\_SC}}$	=	static pressure in the settling chamber of the facility, Pa
p_t	=	total pressure, Pa
q_{dyn}	=	dynamic pressure, Pa
R	=	probe tip radius, m
$\Re$	=	universal gas constant, $m^2/s^2/K$
$T_{\text{s\_Exit}}$	=	static temperature at the nozzle exit of the facility, K
$T_{\text{t\_SC}}$	=	total temperature in the settling chamber of the facility, K
t	=	time, s
$U(t)$	=	instantaneous velocity, m/s
α	=	pitch angle, deg
β	=	yaw angle, deg
γ	=	specific heat ratio for air, $= 1.4$
θ	=	cone angle and θ coordinate measuring from the stagnation point, deg
ρ	=	density, kg/m^3
ϕ	=	roll angle, deg

Received 6 June 2002; accepted for publication 7 July 2004.

*Postdoctoral Research Associate, Department of Aerospace Engineering. Member AIAA.

†Associate Professor, Department of Aerospace Engineering. Associate Fellow AIAA.

Introduction and Background

MULTIHOLE probes must be calibrated in a steady flowfield to determine the pressure coefficients and polynomial expressions needed to reduce data from unknown steady flowfields.[1–4] However, for fast-response probes intended to measure unsteady flows, steady calibration and data-reduction techniques are not adequate because they ignore unsteady flow effects, such as inertial effects. The background theory for unsteady probe calibration is discussed later. The theoretical model assumes that the shape of the probe tip is a perfect sphere and that the flow is ideal (inviscid). However, as is the case with conventional multihole probes, a fast-response multihole probe's tip is a hemisphere-cylinder and not a sphere. Moreover, because of machining imperfections it is expected that the probe tip is not a perfect hemisphere and that the pressure port locations will have some errors as a result of machining tolerances. Finally, the pressure ports on a real tip have finite sizes and are not geometric points, as assumed by the theoretical model. Considering all of the preceding, a very reasonable question emerges: "Are the theories and techniques developed in Parts 1 and 2 still applicable to a real, fast-response multihole probe operating in realistic unsteady air flows"? To answer this question, it is necessary to 1) develop a real, fast-response, multihole probe and 2) develop a facility that can produce unsteady/fluctuating airflows with accurately known instantaneous total and static pressures, velocity magnitude, and angularity and with quantifiable, nonnegligible inertial effects. After this infrastructure is developed, the theories and techniques have to be validated. The velocity magnitude prediction technique was validated in the experiment described in Ref. 2, but, because of the lack of sufficient number of pressure ports on the spherical probe, the flow-angle prediction technique could not be validated. The present work addresses and resolves all of the preceding issues.

As just discussed, it was necessary to develop an unsteady flow facility with accurate and repeatable quantities of velocity magnitude and angularity, total and static pressures, and oscillation frequency. Development of such a facility is challenging and has been attempted by several researchers. Davis and Zasimowich[5] and Schutte et al.[6] developed oscillating pressure calibration systems with frequency range up to 10 kHz, but these were primarily concerned with the production of a fluctuating pressure, not fluctuating velocity. Such

a facility would not be enough for our purposes because the unsteady effects of importance in our work are inertial effects caused by temporal variations of the flow velocity magnitude. Of course, because the pressure transducers in a probe do not discriminate between pressure fluctuations caused by inertial effects and those caused by static-pressure fluctuations (for example acoustic pressure fluctuations), it is important to know which component of the pressure fluctuations is a result of inertial effects (i.e., velocity magnitude fluctuations) and which component is a result of static-pressure fluctuations. This is discussed in more detail later. Kovasznay et al.[7,8] developed a jet facility with two nozzles connected to the same air supply. A spinning perforated disk at the exit of the first nozzle generated a periodic variation in the static pressure upstream of the nozzles resulting in an oscillating velocity at the exit of the second nozzle. For their experiments, the mean velocity was 20 m/s, the oscillation amplitude was approximately ±15%, and oscillation frequencies up to 500 Hz could be generated. A large number of averages (1000–2000) were performed to reduce the random fluctuations in the jet, and the resulting velocity was sinusoidal in nature.

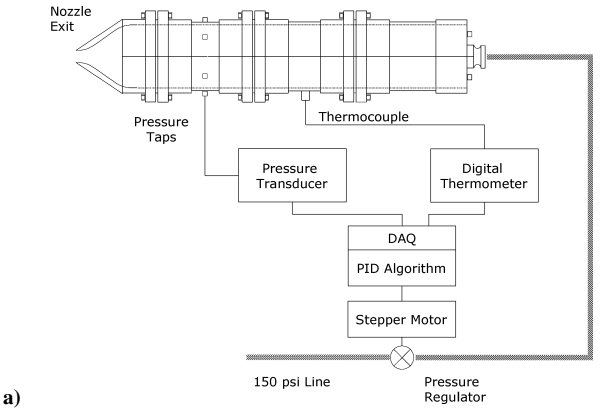

a)

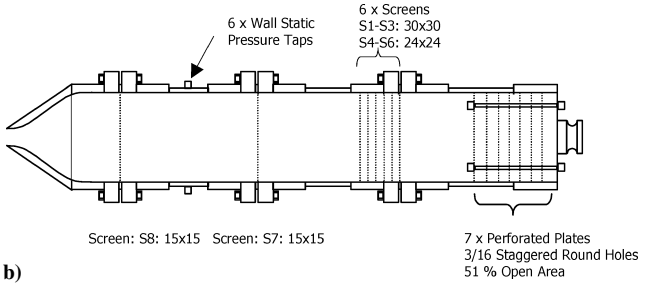

b)

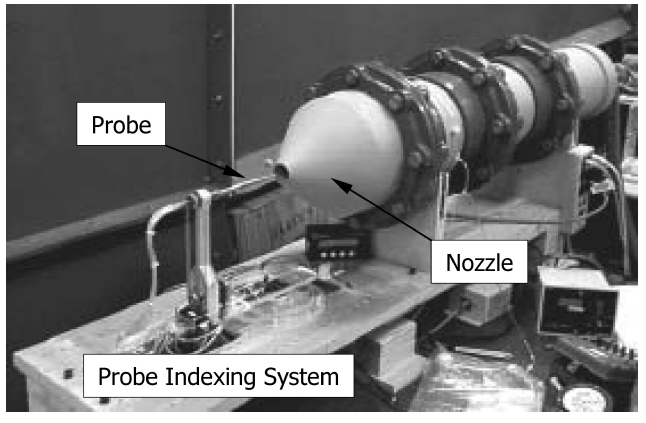

c)

Fig. 1 Schematic of the probe calibration facility, showing control of flow rate, measurement of flow quantities, geometric characteristics, and placement of flow conditioning devices, such as screens and perforated plates (a and b); c) picture of probe calibration facility.

Kovasznay et al.'s[7,8] design was based on an indirect pulsation of the flowfield. The approach taken here uses a direct flow pulsation technique that was intended on extending the maximum attainable velocity and frequency beyond Kovaznay's approach. Initially a steady calibration jet facility, shown in Fig. 1, was developed and then modified for unsteady calibration. A flow pulsation device was designed to fit at the facility's nozzle exit. The pulsation was generated by periodically restricting the cross-sectional area of the jet. The facility can generate repeatable fluctuating flows at frequencies up to 1500 Hz with a mean velocity up to Mach 0.3 and oscillation amplitudes up to 30% of the mean velocity.

Kovasznay et al.[7,8] determined the unsteady pressure coefficient for a sphere in an unsteady axisymmetric flowfield to be a function of the angular position from the stagnation point. Kovaszany showed the maximum value of the unsteady coefficient (a value of three) was found at the forward stagnation point and was based on a modified potential flow solution in an oscillating airflow with finite wavelength. This value was found to deviate from the classical solution (for infinite disturbance wavelength) by a factor of three at the forward stagnation point. As shown in Part 2 (Ref. 2) of this series, the experimental data for the unsteady pressure coefficient follow unsteady potential theory very well. This effort will provide additional experimental proof that this is the case for realistic unsteady airflows using fast-response multihole probes.

In addition to developing the unsteady jet facility, a fast-response multihole probe was developed to validate the theories and algorithms described in Part 1. We developed a five-hole, embedded-sensor, fast-response probe, by embedding five fast-response pressure sensors inside the hemispherical tip of the probe. By embedding the sensors so close to the tip surface, we eliminated problems with tubing frequency response that have plagued other efforts.[7,8]

Basic Calibration Facility

For steady probe calibration, a uniform jet of air with accurately known properties is required. Such a facility was designed for calibration of a wide range of probe types. A schematic of the facility is shown in Fig. 1. The airflow is provided by a 150-psi pressure system, consisting of a 2000-gal surge tank and a two-stage reciprocal compressor, driven by a 100-hp electric motor. An air filtration and drying system was in place to achieve a maximum design flow rate of 270 standard cubic feet per minute (0.13 m^3/s). The pressure is controlled and monitored using a PID-controlled pressure regulator and closed-loop feedback from the settling chamber pressure. A precision pressure transducer (range ±100 torr, ±0.05% full-scale accuracy) was connected to six circumferential pressure taps to eliminate possible static-pressure spatial variations in the settling chamber (Fig. 1b). A thermocouple in the settling chamber measures the flow stagnation temperature and is monitored by the DAQ system. The 8-in. (203-mm)-diam settling chamber facilitated the placement of screens and perforated plates required to create a uniform, low-turbulence jet (Fig. 1b). Seven perforated plates were placed at the inlet of the settling chamber to obtain flow uniformity without the use of a traditional diffuser. These plates are spaced 1 in. apart and have 3/16-in. hole patterns with an effective open area of 51%. The screen spacing and screen mesh were based on the experimental results of Loerke and Nagib.[9] The critical screen Reynolds number, turbulence decay, and critical length scales resulted in screen spacing of 1 in. for six screens having a mesh of 30×30 and 24×24.

The nozzle (contraction) profile is described by a third-order polynomial, where the length of the nozzle is equal to the nozzle inlet diameter. The slope of the profile is zero at the inlet and the exit of the nozzle. Given these boundary conditions, the expression for the curve is given by

$$y(x) = r_1 + \tfrac{3}{4}\left[(r_2 - r_1)/r_2^2\right]x^2 - \tfrac{1}{4}\left[(r_2 - r_1)/r_2^3\right]x^3 \qquad (1)$$

where the definitions of r_1 and r_2 are given in Fig. 2. The contraction ratio for this nozzle is 28.4.

Probe calibrations for this study require the acquisition of data from a wide range of angle inclinations, typically taking several

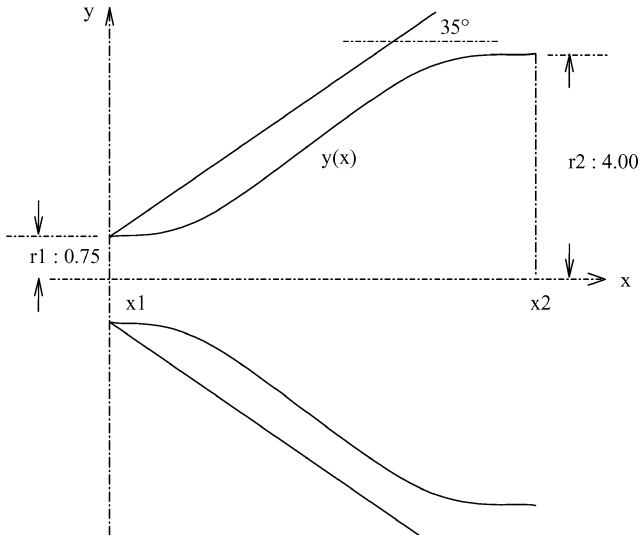

Fig. 2 Nozzle contraction geometry (dimensions in inches).

hours to complete, during which the jet velocity has to be maintained constant (within ±3%), in order to avoid introducing Mach- or Reynolds-number effects into the calibration data. The jet was designed for low-speed calibrations, and a nozzle-exit diameter of 38.1 mm (1.5 in.) was consequently chosen, yielding a maximum sustainable flow speed of Mach = 0.3. Some probe calibrations require a larger velocity range. Therefore, for these cases an extension nozzle was designed to further decrease the nozzle-exit diameter to 25.4 mm (1 in.), yielding a maximum sustainable flow speed of Mach = 0.7. For the present work, the extension nozzle was not used because the velocity range available with the regular 38.1 mm nozzle was sufficient.

The 28:1 contraction ratio ensures that the settling chamber velocity is low (<3.5 m/s for jet exit Mach = 0.3). For these conditions it is assumed that the stagnation pressure in the chamber is nearly identical to the static pressure measured from the six pressure taps. If one further assumes that the discharge coefficient of the nozzle is 1.0, the stagnation pressure at the jet exit equals the stagnation pressure in the settling chamber. Additionally, the nozzle is adiabatic such that the stagnation temperature at the exit equals the measured stagnation temperature in the settling chamber. Using perfect-gas laws for air, the Mach number at the exit can be found from

$$M = \left\{5\left[(p_{s\_SC}/p_{s\_Exit})^{\frac{2}{7}} - 1\right]\right\}^{\frac{1}{2}} \tag{2}$$

The static pressure at the exit p_{s_Exit} is the ambient pressure. The static temperature at the exit is found from

$$T_{s\_Exit} = T_{t\_SC}(p_{s\_Exit}/p_{s\_SC})^{\frac{2}{7}} \tag{3}$$

The velocity at the exit is then given by

$$U = M\sqrt{\gamma \Re T_{s\_Exit}} \tag{4}$$

The facility's flow quality was studied by hot wire (turbulence intensities) and a miniature pitot tube (flow uniformity). Details can be found in Ref. 8. The coordinate system used for the flow survey is shown in Fig. 3a and is consistent with the Cartesian coordinate system used in probe calibration. The flowfield was traversed in the yz plane at constant flow velocity. Several planes were measured between x/d (x measures from the nozzle-exit plane, and d is the nozzle-exit diameter) of 0.1 and 2.5. Figure 3b shows the distribution of the flow stagnation pressure relative to the settling chamber stagnation pressure, at three such planes for $x/d = 0.1$, 0.5, and 1.0 for an exit Mach number of 0.2.

The cone-roll probe-positioning system, otherwise referred to as the probe indexing system, utilizes two stepper motors to control the cone θ and roll ϕ angles of the probe. Figure 4 shows a schematic of the cone-roll mechanism illustrating the different components

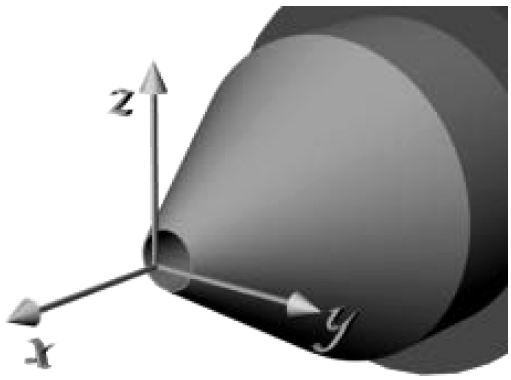

Fig. 3a Coordinate system for facility flow survey.

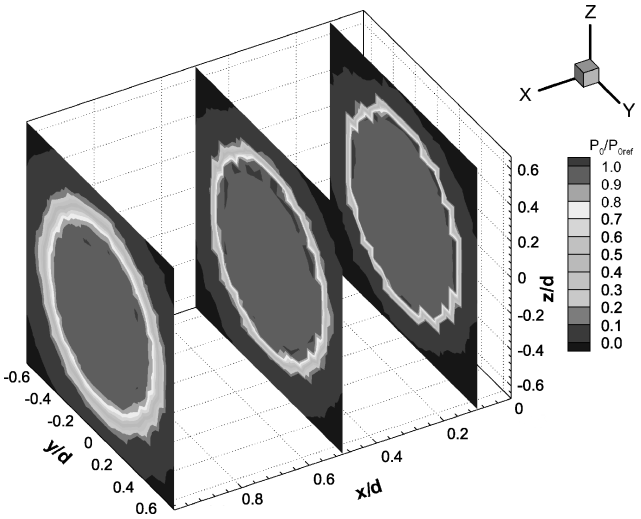

Fig. 3b Cross-sectional total pressure distribution (referenced to the settling chamber stagnation pressure) at $x/d = 0.1$, 0.5, and 1.0 for Mach 0.2.

as well as a picture of the mechanism. The definition of the cone-roll and pitch-yaw angle systems was introduced in Fig. 3 of Part 1. However, for completeness this figure is also included here (Fig. 4c). Both stepper motors have a resolution of 1.8 deg. The roll motor is driven directly, whereas the cone/yaw motor is geared with a 1:50 gearbox, resulting in a cone/yaw positioning resolution of 0.036 deg. The maximum cone angle is approximately 140 deg. Using an extension nozzle, this angle can be increased to about 150 deg, which is suitable for high-angle calibration of omniprobes. Both motions (cone and roll) are monitored by optical encoders, resulting in a positioning accuracy of 0.01 deg or better.

Capitalizing on the ability to traverse the probe with high accuracy, the pitch and yaw angularity of the steady flow at the nozzle exit was determined using a conventional five-hole probe and a "flip-over" technique. The probe is placed in the flowfield with its axis aligned with the geometric axis of the facility's contraction and nozzle. The probe is then coned/yawed to positive and negative yaw angles, and the port pressures and the yaw angle are recorded for each yaw location. The probe is then rolled 180 deg, and the yawing procedure is repeated. A pressure coefficient is defined to nondimensionalize the measured pressures from ports 1, 2, and 3:

$$Cp = \frac{p_2 - p_3}{p_1 - \frac{1}{2}(p_2 + p_3)} \tag{5}$$

The port numbering is shown in Fig. 5a. The pressure coefficient is calculated for all of the test points (at 0- and 180-deg roll positions) and plotted vs yaw angle (Fig. 5b). Figure 5b reveals that the two curves, for 0- and 180-deg roll, respectively, intersect at a yaw angle not exactly equal to zero. The specific yaw angularity is 0.06 deg. To determine the pitch-angle offset, the Cp curve for roll = 0 deg is first curve fitted to give an expression of the yaw angle vs Cp:

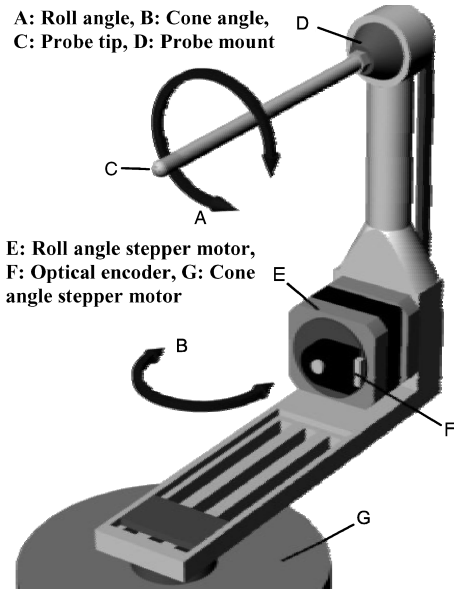

Fig. 4a Schematic of probe positioning/indexing system.

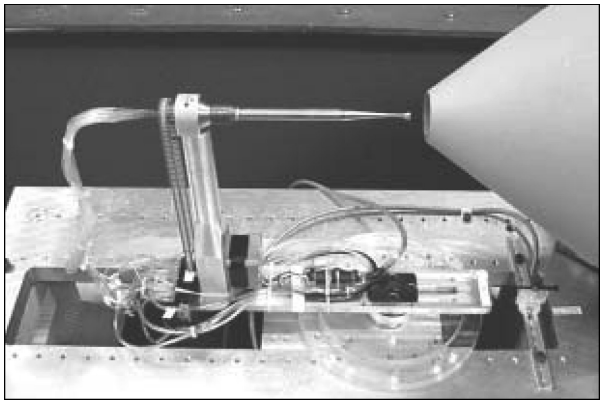

Fig. 4b Probe positioning/indexing system.

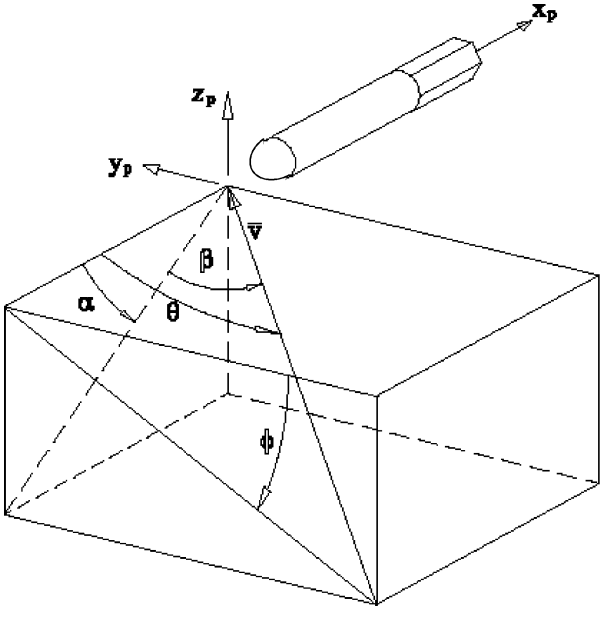

Fig. 4c Angle.

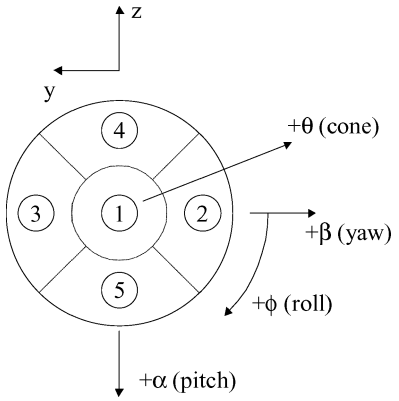

Fig. 5a Port numbering definition.

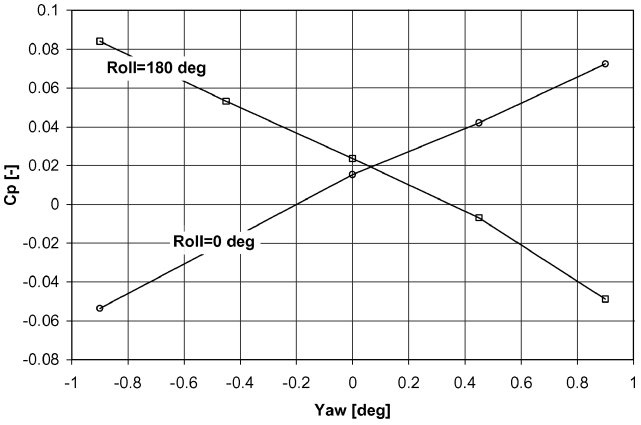

Fig. 5b *Cp* vs yaw angle for 0- and 180-deg roll. The yaw flow angularity is 0.06 deg.

$\beta = \beta(Cp)$. The probe is then rotated to the zero yaw angle, rolled 90 deg, the port pressures are recorded, and the *Cp* coefficient calculated. The pitch-angle offset is then calculated from the expression $\beta = \beta(Cp)$. The specific pitch angularity was found to be 0.04 deg. The yaw-angle misalignment is corrected by properly realigning the cone-roll mechanism. Such realignment is not possible in the pitch direction using this mechanism. Instead, the pitch-angle misalignment is corrected for in a postcalibration procedure using the method outlined by Zeiger and Schaeffler,[10] as follows. First the velocity components are calculated in the probe-fixed coordinate system:

$$u_p = U\cos\theta\cos\beta$$

$$v_p = U(-\cos\phi\sin\theta\cos\beta + \sin\phi\sin\beta)$$

$$w_p = U(\sin\phi\sin\theta\cos\beta + \cos\phi\sin\beta)$$

where θ and ϕ are traversed by the probe-positioning system and β is the pitch-angle offset. Then the true cone and roll angles θ_n and ϕ_n (corrected for the pitch angle offset) are solved for, from the following equations:

$$u_p = |U_p|\cos\theta_n, \qquad v_p = |U_p|\sin\theta_n\cos\phi_n$$

$$w_p = |U_p|\sin\theta_n\sin\phi_n$$

where

$$|U_p| = \sqrt{(u_p)^2 + (v_p)^2 + (w_p)^2}$$

Flow Pulsator

Based on the steady calibration jet facility just described, the flow pulsation device was designed to fit at the nozzle exit. The pulsation was generated by periodically restricting the cross-sectional area of the jet. Figure 6 presents the conceptual design of the flow-pulsator.

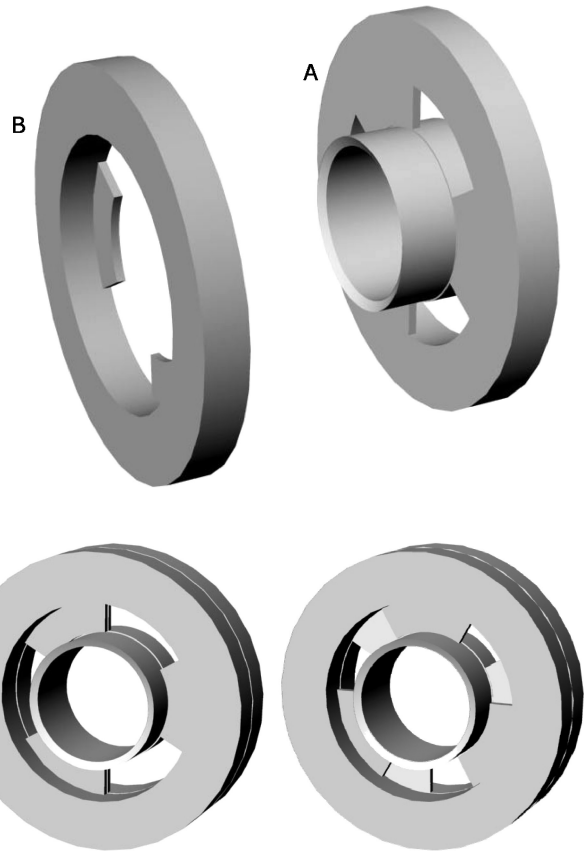

Fig. 6 Exploded (top) and assembled view of the flow-pulsator at two different rotor positions (bottom): A, stator and B, rotor.

The assembly consists of a stator with a short tube mounted at its center and a rotor mounted 0.5 mm downstream of the stator (items A and B in Fig. 6, respectively). On both the stator and rotor, three "teeth" protrude into the flow. When the rotor rotates, the device generates a periodic restriction of the flow-path area. From left to right, the bottom of Fig. 6 shows the most open position, followed by clockwise rotation of the rotor and a partial restriction of the area. Figure 7 shows a photograph of the flow-pulsator, illustrating the most open position (Fig. 7a), the most closed position (Fig. 7b), and the positioning of the probe in front of the flow-pulsator (Fig. 7c). The flow-pulsator device attaches right at the tip (exit) of the facility nozzle.

The rotor is mounted in a 70-mm ball bearing and driven by an electric motor. The rotational speed can be varied accurately from 0 to approximately 500 Hz, yielding 0- to 1500-Hz flow pulsation. The maximum sustained mean or peak velocity range of the jet with the flow-pulsator is approximately Mach 0.5. The flow-pulsator is phase referenced using an optical encoder, such that consecutive tests at identical conditions can be performed and compared in corrected phase. The central tube is 22.1 mm in diameter, and the outer diameter of the flow-pulsator is 38.1 mm, which gives a maximum change in area of 45%.

Instrumentation

To quantify the flow time-varying flow characteristics of the calibration facility, several different instruments were used, including hot-wire anemometry to measure the instantaneous velocity magnitude, a fast-response static-pressure probe, and a five-hole fast-response pressure probe. The hot-wire system was used to measure the axial velocity fluctuations and served as the reference for the velocities predicted by the fast-response, five-hole probe. A fast-response static-pressure probe was used to measure the fluctuating static pressure. The instantaneous static pressure at the measurement point is the sum of the mean ambient pressure and the static-pressure fluctuations generated by the flow-pulsator. The contribution from

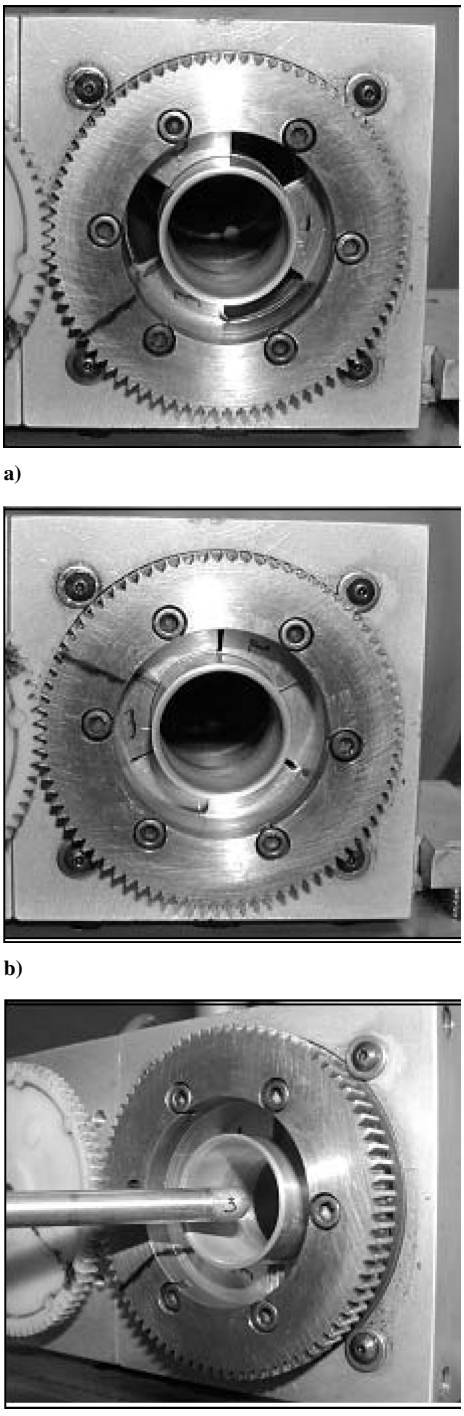

a)

b)

c)

Fig. 7 Pictures of flow-pulsator: a) fully open, b) fully closed, and c) pulsator with fast-response five-hole probe mounted at the nozzle exit.

the rotation of the flow-pulsator pressure was significant and was measured using a fast-response, static-pressure probe. This probe (Fig. 8) incorporates an Entran EPE-541-2P pressure transducer with a range of ± 2 psi and a frequency response of 20 kHz. Eight circumferential ports on the probe forebody are located approximately two diameters downstream of the tip (Fig. 8). The probe was placed at the same location as the fast-response, five-hole probe, such that the measured static pressure is the same as that sensed by the fast-response, five-hole probe. The recorded static pressure itself is not constant but has fluctuations introduced by the rotation of the flow pulsator. The static probe recorded a small mean decrease in the static pressure for increasing flow speeds as a result of the pressure distribution on the probe forebody. To keep the probe

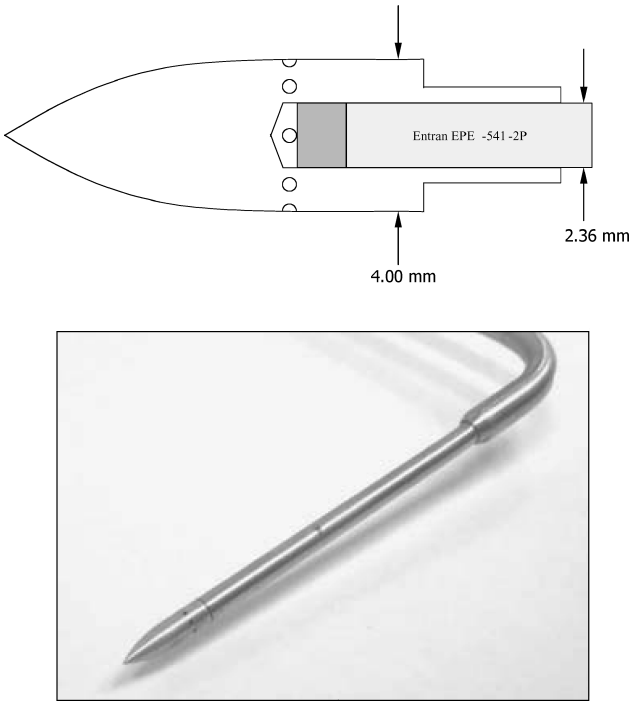

Fig. 8 Fast-response static-pressure probe.

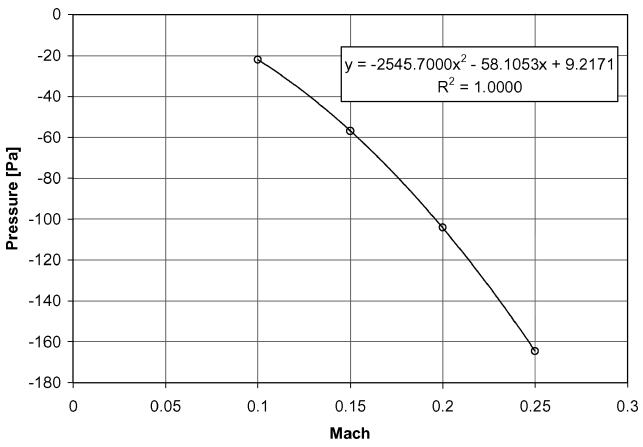

Fig. 9 Recorded pressure vs Mach number for static-pressure probe.

short, the placement of the static-pressure holes was moved forward of the ideal location where the static pressure would asymptote to freestream static pressure. To account for this decrease, the static-pressure probe was calibrated vs Mach number in the facility, in a steady flow, that is, with the flow-pulsator off. This decrease was characterized and used to correct the recorded pressure (Fig. 9). It should be emphasized that for physical understanding of the calibration process we have used a separate static-pressure probe (besides the fast-response, five-hole probe); this does not mean that the five-hole probe cannot be used by itself for the determination of the instantaneous flow velocity and angles. Later we discuss the technique that enables a fast-response, five-hole probe to operate by itself, without the need for a separate static-pressure probe.

A fast-response, five-hole probe was designed to test the unsteady probe calibration routines. This probe incorporates five unsteady pressure transducers (Kulite XCS-062-5D) mounted in the probe tip. A conceptual drawing and photograph of the probe are shown in Fig. 10. The hemisphere tip diameter of this probe is 6.35 mm with a tolerance of ±0.01 mm. The sculptured silicon diaphragm has a natural frequency of 150 kHz, and the rated usable frequency response is 20 kHz. The pressures from both the static-pressure probe and the five-hole probe were amplified using Entran

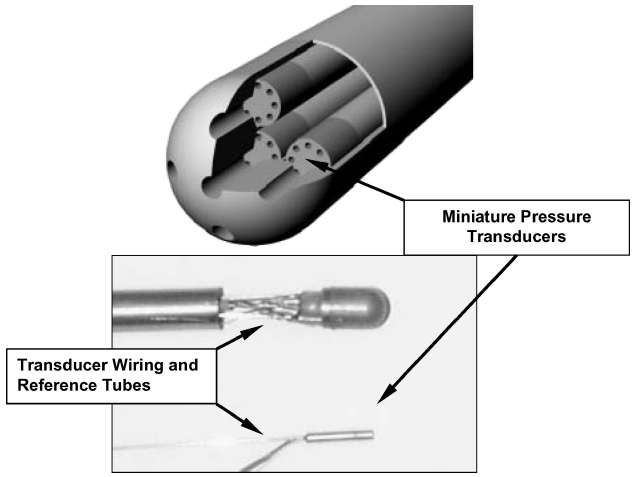

Fig. 10 Cross-sectional view and picture of the 6.35-mm, five-hole, fast-response probe. The probe has five Kulite XCS-062 transducers embedded in the tip. Lower picture also shows a stand-alone Kulite for size comparison.

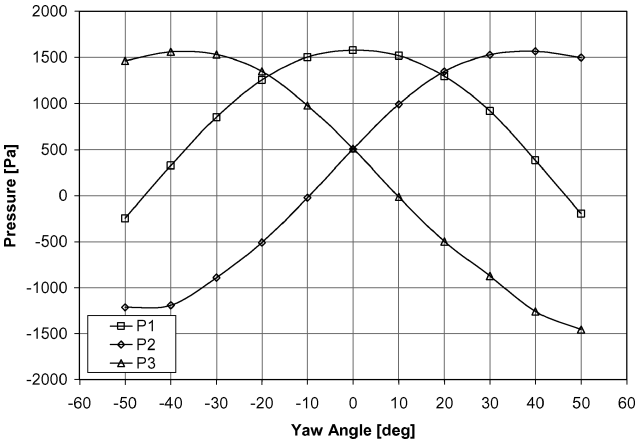

Fig. 11 Steady port pressures vs yaw angle, for the fast-response, five-hole probe.

IMV-15 amplifiers at a gain of 100. The data were acquired using a simultaneous sample and hold A/D converter (National Instruments AT-MIO-16E-1 and SC2040) at frequencies up to 100 kHz and a 12-bit resolution.

Results and Discussion

Steady Probe Calibration

To simplify the discussion of the calibration process, only ports 1 to 3 will be used corresponding to the yaw calibration portion of the total process. The roll angle is set to zero such that the yaw angle is set directly by the arm of the cone-roll traversing system. The probe (shown in Fig. 10) was calibrated from −50 to +50 deg in yaw angle in 10-deg increments. At each location, the port pressures (for ports 1–3) were recorded and are shown in Fig. 11. Excellent symmetry is seen for all ports.

For each angle, the pressure coefficient B_β was calculated from Eq. (6):

$$B_\beta = \frac{p_2 - p_3}{p_1 - \frac{1}{2}(p_2 + p_3)} \tag{6}$$

This definition should only be used when the central port has the highest pressure, and this is true for yaw angles below approximately 20 deg (for pitch = 0). Figure 12 shows the curve-fitted yaw angle vs the pressure coefficient for the range of ±20 deg in yaw. The velocity prediction routine requires a second steady pressure coefficient to

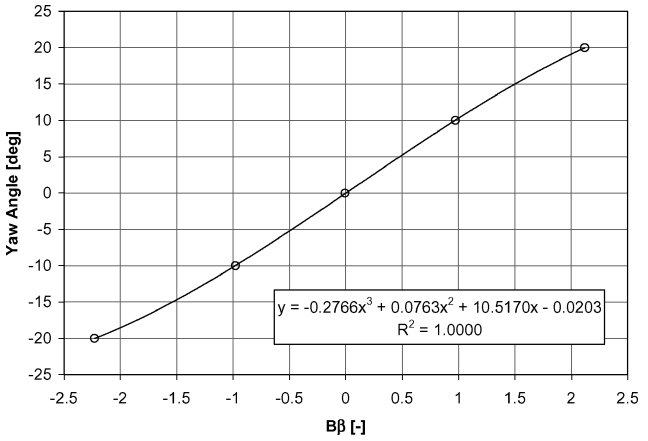

Fig. 12 Curve fit of yaw angle vs B_β for yaw angle β in the range of ± 20 deg.

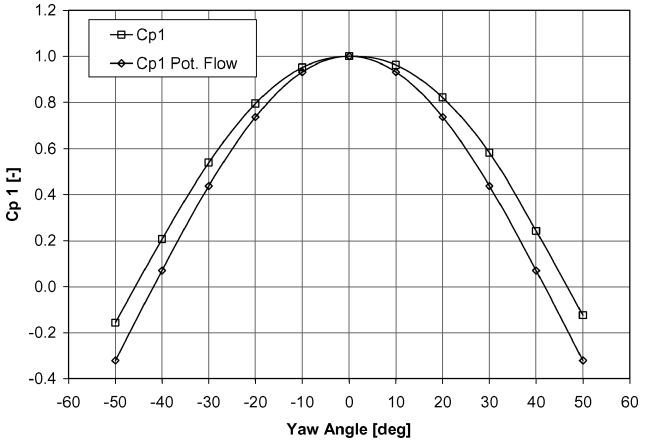

Fig. 13 Steady pressure coefficient based on the central port.

be defined. For the central port this coefficient is defined as

$$Cp_{\text{STEADY}_1}(\alpha, \beta) = \frac{p_1(\alpha, \beta) - p_s}{\frac{1}{2}\rho U(t)^2} \tag{7}$$

For these tests, the pitch angle α is always 0 deg. A plot of this coefficient Cp_{STEADY_1} is shown in Fig. 13. This also compares the measured results to the steady pressure coefficient based on potential flow over a sphere. Although the trends are the same, the experimental curve is consistently higher at yaw angles different from zero. This is because the actual probe is not a sphere, but rather a hemisphere-cylinder. The steady pressure coefficient for the central port was curve fitted to give an explicit polynomial expression vs the yaw angle.

Unsteady Probe Calibration

The experimental determination of the unsteady pressure coefficient Cp_U is more challenging than the steady pressure coefficient. The theoretical potential flow over a sphere predicts a Cp_U coefficient of 1.0 at the stagnation point, which should also be the value of Cp_U at the stagnation point over a hemispherical tip probe at zero incidence angle. A combined theoretical and experimental study undertaken by Kovasznay et al.[7,8] found that this coefficient for a sphere should be 3.0 at the forward stagnation point. Our findings do not agree with these values. An explanation regarding the discrepancy in Kovasznay et al.[7,8] is based on the fact that they forced matching of the experimentally measured pressures to their theory to derive expressions for the transfer function of their tubing-transducer system. [See Part 2 (Ref. 2) for a more detailed discussion of their approach.] To determine Cp_U experimentally, the probe must be inserted into a flowfield with known flow angularity and velocity. In addition, the flowfield must be fluctuating or have a controlled acceleration that yields a significant nondimensional acceleration K. Although derived in Part 1 (Ref. 1), the related formulas are reiterated here for completeness:

$$\frac{p(\alpha, \beta, t) - p_S}{1/2\rho U(t)^2} = Cp(\alpha, \beta, t)$$

$$\equiv Cp_{\text{STEADY}}(\alpha, \beta) + Cp_{\text{UNSTEADY}}(\alpha, \beta, t) \tag{8}$$

or

$$Cp(\alpha, \beta, t) = Cp_S(\alpha, \beta) + K(t)Cp_U(\alpha, \beta) \tag{9}$$

where

$$Cp_{\text{STEADY}} = Cp_S, \qquad Cp_{\text{UNSTEADY}} = K(t)Cp_U$$

$$K(t) = \frac{R}{U(t)^2}\frac{\mathrm{d}U(t)}{\mathrm{d}t} \tag{10}$$

Moreover, for flow over a sphere (potential flow)

$$Cp_S = \left[\tfrac{9}{4}\cos^2(\theta) - \tfrac{5}{4}\right], \qquad Cp_U = \cos(\theta) \tag{11}$$

By combining Eqs. (8–10), the unsteady pressure coefficient for each port can be found from

$$Cp_{U_i}(\alpha, \beta) = \left[\frac{p_i(\alpha, \beta, t) - p_s}{\frac{1}{2}\rho U(t)^2} - Cp_{S_i}(\alpha, \beta)\right] \Big/ K(t) \tag{12}$$

Again, only the pressure coefficient for the central port is needed to resolve the velocity magnitude. The numerator in Eq. (12) will tend to zero for negligible inertial effects (as will the denominator for steady flow). This is why, if a periodically varying flowfield is used to calculate Cp_U, its parameters must be such that significant inertial effects are manifested. Moreover, special caution must be exerted to ensure that only data points where the numerator and denominator of Eq. (12) have significant magnitudes (for example, the peaks and valleys of the velocity-vs-time graph, where $\mathrm{d}U/\mathrm{d}t$ is small or zero, must be avoided). Theoretically, any data point in the time series, except where $\mathrm{d}U/\mathrm{d}t$ is zero, can be used to determine Cp_U. However, in the vicinity where $\mathrm{d}U/\mathrm{d}t$ is small differences between the measured and the true pressure are also small. There is always uncertainty and noise in measured data. Therefore, one should avoid these parts of the curves and instead use a conditional approach where both the numerator and denominator have significant values. Technically, only one point is required to estimate Cp_U; however, because of experimental errors, averaging the data over a number of points is recommended. In Fig. 14, a theoretical sinusoidal velocity signal is presented, and the nondimensional acceleration K is calculated. In the figure, $P(t)$ is the true flow dynamic pressure, whereas $P1(t)$ is be the pressure that would be measured at the stagnation point of a theoretical spherical probe, according to unsteady potential flow theory. Only data points where the magnitude of K is significant (inside the two rectangles) should be considered. The predicted Cp_U for each such point can be calculated and averaged. The procedure should be repeated for all flow incidence angles.

From the preceding discussion and the fact that for the optimal facility operating conditions the K value is only around 3.3% or 0.033, it is obvious that accurate experimental determination of the unsteady pressure coefficient for the specific probe is beyond the capabilities of the facility. Instead, guided by our findings in Part 2, a theoretical model was chosen. Two models were considered: the first is based on the classic potential flow solution over a sphere, and the second is based on Kovasznay et al.'s solution.[7,8]

Unsteady Flow Measurements and Flow Angle and Velocity Predictions

The measurement plane was set 5.1 mm inside the inner tube of the flow pulsator (the tube is illustrated in A of Fig. 6), where a clean velocity signal was observed. The pulsation frequency and velocity

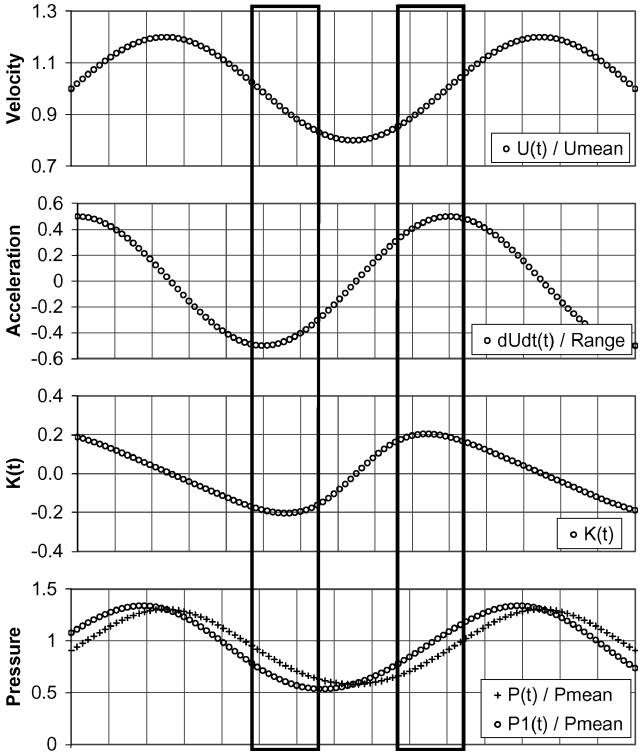

Fig. 14 Selection of data for determining the unsteady pressure coefficient.

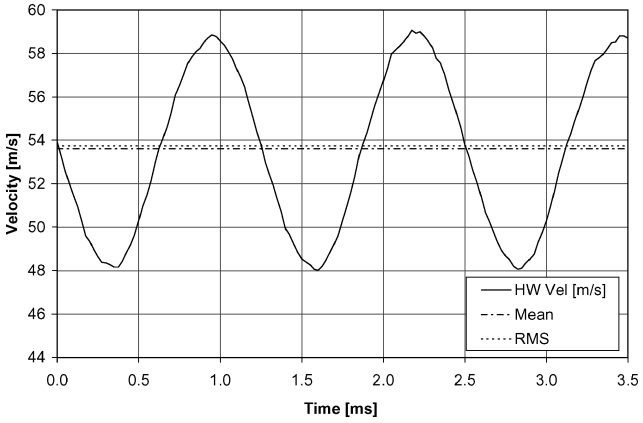

Fig. 15 Velocity measured by hot wire for mean flow speed $M = 0.15$ and frequency $f = 800$ Hz.

must be set such that the nondimensional acceleration K is maximized to ensure large, and thus measurable, inertial effects for the five-hole probe. Large K values are achieved by a combination of large fluctuation amplitude, high frequency, and the lowest possible velocity. In the unsteady calibration facility the best combination of flow speed and pulsation actuation frequency to maximize the value of K, while achieving a clean velocity time trace, was found to be a mean Mach number of 0.15 and a pulsation frequency of 800 Hz corresponding to $K = \pm 0.03$. The unfiltered, hot-wire velocity is shown in Fig. 15 for $M = 0.15$, $f = 800$ Hz. Figure 16 shows higher harmonics are present, but their magnitudes are at least one-and-a-half orders of magnitude smaller than the magnitude of the fundamental. It is important to reiterate how difficult it is to experimentally obtain such a clean velocity signal with significant amplitude and at these fluctuation frequencies. The present flow-pulsator is the fourth design in a series of flow-pulsation mechanisms that we designed, built, and tested.

Three separate tests were required to measure the flowfield with the hot-wire system, the static-pressure probe, and the fast-response

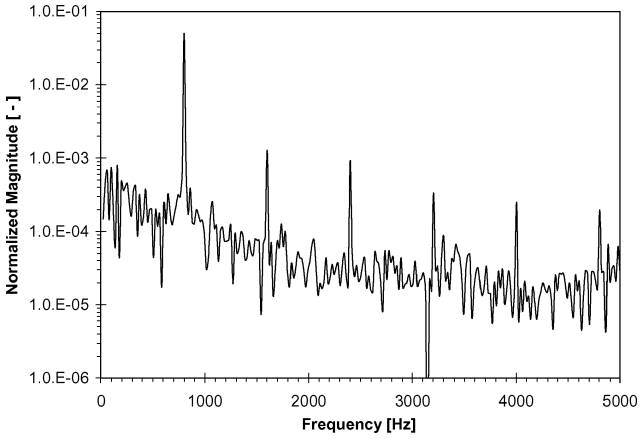

Fig. 16 Normalized spectrum magnitude for the hot-wire velocity in Fig. 16.

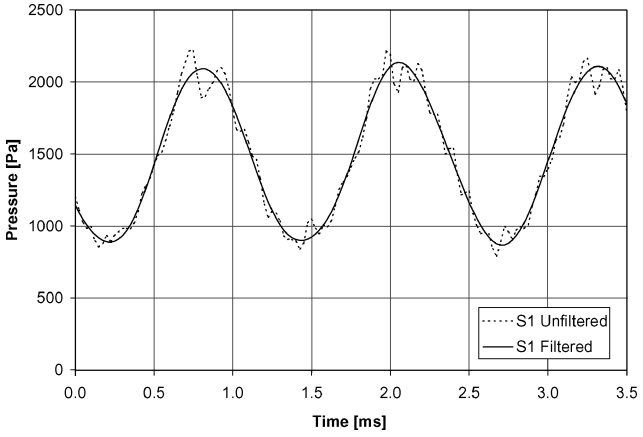

Fig. 17 Unfiltered and filtered five-hole probe center port pressure, for mean flow speed $M = 0.15$ and frequency $f = 800$ Hz.

five-hole probe. The flow-pulsator frequency was set to 800 Hz for each test. The nondimensional acceleration was calculated from the hot-wire velocity, based on the five-hole probe tip diameter, and its maximum and minimum values were ± 0.033 or 3.3%. For all measurements the optical encoder signal was recorded and enabled consecutive measurements to be phase referenced to the velocity measured with the hot wire. The yaw angle of the five-hole probe was set to -10 deg, and a time series of pressures was recorded. All channels were sampled simultaneously at 80 kHz, providing 100 samples per period. A total of 8192 points was sampled yielding 81 full periods in the data set. The data were low-pass filtered with a cutoff frequency equal to three times the pulsator frequency, that is, 2.4 kHz for the present test case. Example test data are shown in Fig. 17, for a yaw angle of -10 deg. The unfiltered and filtered center port pressures are shown.

The fluctuating static pressure is seen equally by all ports on the five-hole probe. Therefore it will cancel out in the differential definition of the independent coefficients B_α and B_β. In addition, it was shown in Part 1 that the inertial effects will nearly cancel out in B_α and B_β, and the measured port pressures, without correction for fluctuating static or inertial effects, can be used to accurately predict the flow angle. The predicted yaw angle based on the unfiltered port pressures is shown in Fig. 18. The mean predicted yaw angle is -10.32 deg with a standard deviation of 0.53 deg. Calculating the yaw angle based on the low-pass-filtered port pressures yields a mean angle of -10.31 deg, and the standard deviation drops to 0.28 deg (Fig. 18). The mean offset error is within the prediction capability of the probe (± 0.5 deg), and no further optimization was attempted. The same range of errors in the predicted yaw angle was observed throughout the test range from -20 to $+20$ deg in yaw angle.

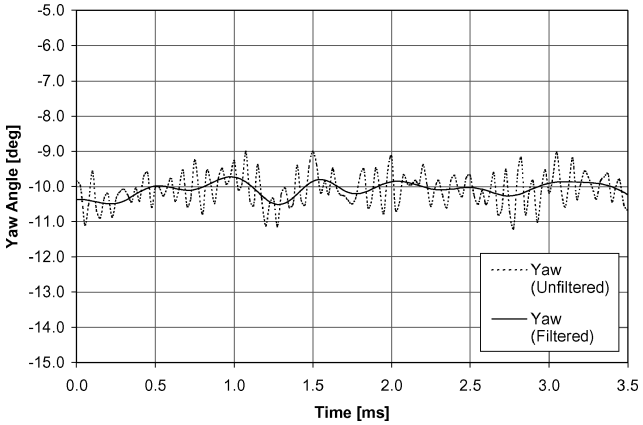

Fig. 18 Predicted yaw angle based on unfiltered and filtered port pressures.

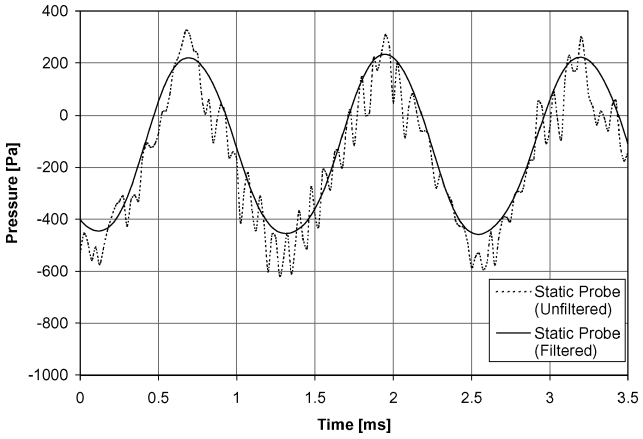

Fig. 19 Unfiltered and filtered corrected static pressure.

Figure 19 shows the static pressure measured with the fast-response static-pressure probe. The measured pressure is filtered and corrected for the mean pressure drop as a function of velocity (Fig. 9). With the assumption that the temperature is constant, the density change is calculated from the fluctuating static pressure based on perfect-gas law, and, for the data in Fig. 19, it was found to be 1.18 kg/m^3 $\pm 0.4\%$.

To accurately predict the velocity magnitude, the measured port pressures must be corrected for the static-pressure fluctuation. There are some low-frequency oscillations present in the flowfield, which call for ensemble averaging over several periods. The ensemble averaging is based on accurate phase referencing using the optical encoder that produces a transistor-to-transistor logic pulse for each revolution of the flow pulsator. Then, calculation of the true velocity magnitude, from the probe measured pressures, is performed using the numerical routine outlined in Part 1 (Ref. 1). The ensemble average of 40 periods of the hot-wire velocity, the velocity predicted by the numerical routine (marked "correction") as well as the velocity predicted by the port pressure without inertial correction (marked "no correction"), are shown in Fig. 20. This figure clearly shows the contribution from the inertial effects. The velocity predicted by ignoring the inertial effects leads the hot-wire velocity in phase and has a slightly larger magnitude. The results from the numerical routine agree very well with the hot-wire velocity.

The numerical routine used to predict the velocity in Fig. 20 was based on experimental determination of the steady pressure coefficient Cp_S while the unsteady pressure coefficient Cp_U was based on potential flow over a sphere [$\cos(\theta)$]. Using the unsteady coefficient definition based on Kovasznay et al.,[7,8] the velocity is overcorrected and appears to lag the hot-wire velocity in phase and have a lower magnitude (Fig. 21).

The errors (difference to the hot-wire velocity) of the corrected and uncorrected flow velocity are shown in Fig. 22. Without any

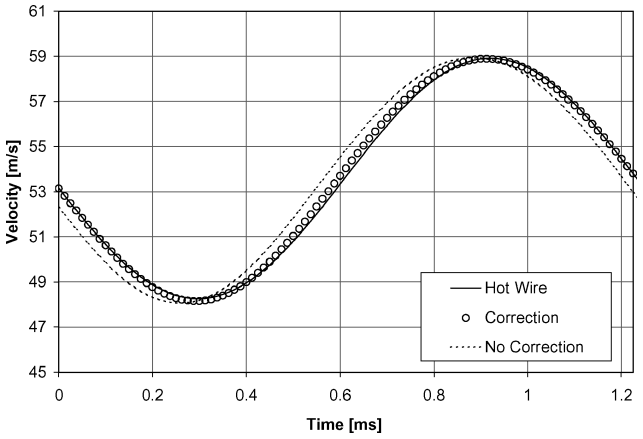

Fig. 20 Ensemble-averaged velocity from hot-wire, numerical correction routine, and center port pressure without inertial effect correction.

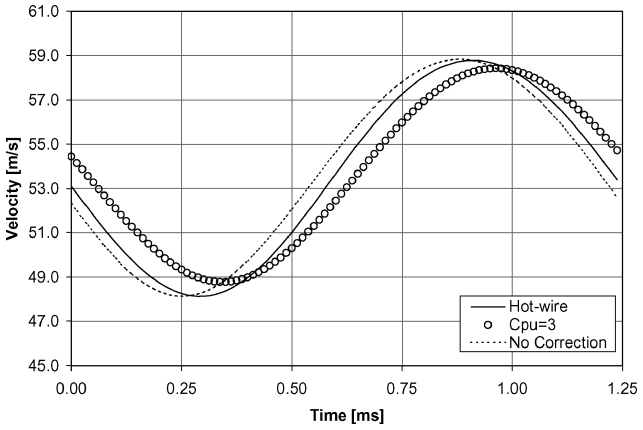

Fig. 21 Exact and predicted velocity based on the unsteady coefficient of Kovasznay et al.[7,8]

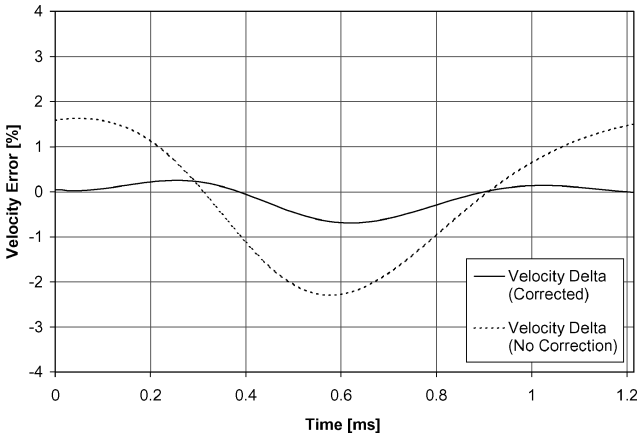

Fig. 22 Velocity prediction error (difference to hot-wire velocity), in percent, from numerical correction method and from uncorrected center port pressure.

inertial effect correction the mean absolute error is 1% with a standard deviation of 1.24%. The corrected data have a mean absolute error of -0.15% and a standard deviation of 0.18%. The error in the predicted dynamic pressure if the inertial effects are not accounted for, should, equal the value of $K \times Cp_{\text{unsteady}}$. The value of K was calculated from the hot-wire velocity, and the prediction results in Fig. 20 were converted to dynamic pressure. Figure 23 shows the prediction errors in dynamic pressure based on the corrected and uncorrected velocity predictions. The uncorrected error follows very nearly the value of $K \times Cp_{\text{unsteady}}$ as expected. The discrepancy in

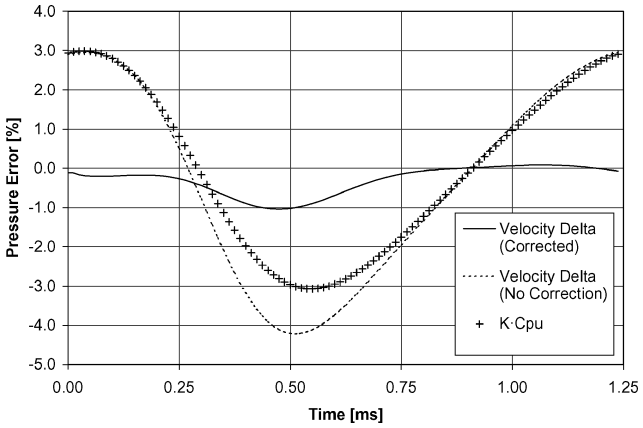

Fig. 23 Ensemble-averaged dynamic pressure error for the numerical correction method, no correction, and ensemble-averaged nondimensional acceleration based on hot-wire velocity.

the valley is the result of the experimental uncertainty, and by adding the errors from the corrected prediction (Fig. 22) and $K \times Cp_{\text{unsteady}}$ the uncorrected error is obtained.

The same velocity prediction errors were obtained for all test angles in the range of -20 to $+20$ deg in yaw. Similar results were also obtained for other combinations of flow velocity and pulsation frequencies. The details of these tests can be found in Ref. 11. The presented method is restricted to low-angle flows, which is extended to approximately ± 25 deg, but the method can be easily extended to the high-angle range. The magnitude of the unsteady flow effects in the probe calibration facility was moderate. Much larger nondimensional accelerations can be found in practice, for example, in turbomachinery flowfields.

The main concern about the presented procedure is the treatment of the local static pressure. A nonconstant static pressure must be measured accurately in phase and be corrected for. In the pressure coefficients B_α and B_β the inertial contributions in effect cancel out. However, this is not the case in the total and static-pressure coefficients. Common definitions of these coefficients strongly depend on the inertial effects seen by the individual pressure ports and are not readily modifiable to a form where the inertial effects can cancel out. Further study is undertaken to arrive at a modified set of coefficients or correction function based on the port specific unsteady pressure coefficients, in order to also be able to predict the instantaneous static pressure. One apparent way to deal with this issue is to use the pressures not from one port (port 1) but from two ports, for example, ports 1 and 2 and their corresponding steady and unsteady coefficients. The pressures at these two ports are given by

$$p_1(\alpha, \beta, U, t) = p_s + \frac{1}{2}\rho U(t)^2 Cp_{\text{steady\_1}}(\alpha, \beta) + \frac{1}{2}\rho R \frac{\mathrm{d}U(t)}{\mathrm{d}t} Cp_{\text{unsteady\_1}}(\alpha, \beta) \tag{13}$$

$$p_2(\alpha, \beta, U, t) = p_s + \frac{1}{2}\rho U(t)^2 Cp_{\text{steady\_2}}(\alpha, \beta) + \frac{1}{2}\rho R \frac{\mathrm{d}U(t)}{\mathrm{d}t} Cp_{\text{unsteady\_2}}(\alpha, \beta) \tag{14}$$

Because both ports sense the same static pressure p_s, we can eliminate it by subtracting Eq. (14) from Eq. (13):

$$p_1(\alpha, \beta, U, t) - p_2(\alpha, \beta, U, t) = \frac{1}{2}\rho U(t)^2 [Cp_{\text{steady\_1}}(\alpha, \beta) - Cp_{\text{steady\_2}}(\alpha, \beta)] + \frac{1}{2}\rho R \frac{\mathrm{d}U(t)}{\mathrm{d}t} [Cp_{\text{unsteady\_1}}(\alpha, \beta) - Cp_{\text{unsteady\_2}}(\alpha, \beta)] \tag{15}$$

and then rearranging Eq. (15) in a form amenable to the numerical correction technique:

$$\frac{\mathrm{d}U(t)}{\mathrm{d}t} = [p_1(\alpha, \beta, U, t) - p_2(\alpha, \beta, U, t)] \times \frac{2}{\rho R [Cp_{\text{unsteady\_1}}(\alpha, \beta) - Cp_{\text{unsteady\_2}}(\alpha, \beta)]} - U(t)^2 \frac{[Cp_{\text{steady\_1}}(\alpha, \beta) - Cp_{\text{steady\_2}}(\alpha, \beta)]}{R [Cp_{\text{unsteady\_1}}(\alpha, \beta) - Cp_{\text{unsteady\_2}}(\alpha, \beta)]} \tag{16}$$

which can be solved for the velocity $U(t)$. This solution can then be substituted in either Eq. (13) or Eq. (14), and the static pressure p_s can be calculated.

Conclusions

Multihole probes have traditionally been restricted to steady flowfields as a result of several unresolved issues in their response to unsteady flowfields. This work presents the experimental validation of a procedure to quantify and correct for the most important unsteady aerodynamic effect, namely, inertial effects. The present work addresses and answers the following question: "Are the theories and techniques developed in Parts 1 and 2 still applicable to a real, fast-response multihole probe operating in realistic unsteady airflows?" Toward answering this question, two subtasks had to be addressed first: 1) development of a real, fast-response, multihole probe and 2) development of a facility that can produce unsteady/fluctuating airflows with accurately known instantaneous total and static pressures, velocity magnitude, and angularity and with quantifiable, nonnegligible inertial effects. To this end, a test facility was designed and constructed to expose a five-hole, fast-response probe to a known and repeatable unsteady flowfield. This facility provides a jet of air at velocities up to Mach 0.3 and pulsation frequencies up to 1500 Hz. The amplitude of the oscillation depends on both the flow velocity and the frequency of oscillation, but it is in the range of $\pm 20\%$. A fast-response, five-hole probe was also developed.

The experimental data showed that the angle prediction routine yields excellent results independent of the inertial effects and fluctuating static pressure. The present work also validated the fact [discussed in Part 2 (Ref. 2)] that the unsteady pressure coefficient follows potential flow theory quite well, at least in the angularity range of interest here. This is in disagreement with Kovasznay et al.[7,8] At this point, the only possible explanation that we can offer regarding the discrepancy is based on the fact that Kovasznay et al. forced matching of the experimentally measured pressures to their theory in order to derive expressions for the transfer function of their tubing-transducer system. [See Part 2 (Ref. 2) for a more detailed discussion of their approach.]

The presented velocity prediction routine quantifies and corrects for the inertial effects for one pressure port (central) on the probe. For the velocity magnitude prediction, the method assumed that the static pressure is known, but not necessarily constant. The velocity angles prediction does not require the knowledge of the static pressure. The apparent limitation of the technique (i.e., the need to know the static pressure a priori in order to determine the velocity magnitude) was addressed, and the technique was expended such that is can also be applicable to cases where the instantaneous static pressure is not known. However, in these cases the data from one pressure port on the tip are not enough. In these cases, the measured pressures from at least two ports are necessary. Using a fast-response static probe to measure the static-pressure fluctuation, the port pressures at the probe central port were corrected, and excellent prediction in the velocity was demonstrated. The only restriction on the method is that it does not account for significant spatial gradients over the probe diameter. If no significant such gradients exist, the method can predict both the instantaneous flow velocity and angles in unsteady flowfields.

Acknowledgments

This work was sponsored by the Air Force Office of Scientific Research under Grant/Contract F49620-98-1-0162. The authors thank

Thomas Beutner, the Technical Monitor of the project, as well as his predecessor, Mark Glauser. The work was also supported by Aeroprobe Corporation under Project 32500-7260M. The authors also thank Rick Allen for building the probes and support hardware as well as Lance Traub for his guidance in the initial stages of this work.

References

[1]Johansen, E. S., and Rediniotis, O. K., "Unsteady Calibration of Fast-Response Pressure Probes, Part 1: Theoretical Studies," *AIAA Journal*, Vol. 43, No. 4, 2005, pp. 816–826.

[2]Johansen, E. S., and Rediniotis, O. K., "Unsteady Calibration of Fast-Response Pressure Probes, Part 2: Water-Tunnel Experiments," *AIAA Journal*, Vol. 43, No. 4, 2005, pp. 827–834.

[3]Bryer, D. W., and Pankhurst, R. C., "Pressure-Probe Methods for Determining Wind Speed and Flow Direction," Her Majesty's Stationery Office/National Physics Lab., Campfield Press, St. Albans, England, U.K., 1971.

[4]Everett, K. N., Gerner, A. A., and Durston, D. A., "Seven-Hole Cone Probes for High Angle Flow Measurements: Theory and Calibration," *AIAA Journal*, Vol. 21, No. 7, 1983, pp. 992–998.

[5]Davis, P. A., and Zasimowich, R. F., "High Frequency Dynamic Pressure Calibration Technique," Instrument Society of America, Paper 85-0109, 1985.

[6]Schutte, P. C., Cate, K. H., and Young, S. D., "A Dynamic Pressure Calibration Standard," Instrument Society of America, Paper 85-0110, 1985.

[7]Kovasznay, L. S. G., Tani, I., Kawamura, M., and Fujita, H., "Instantaneous Pressure Distribution Around a Sphere in Unsteady Flow," Office of Naval Research, Rept. N00014-67-0163-002, Washington, DC, Dec. 1971.

[8]Kovasznay, L. S. G., Tani, I., Kawamura, M., and Fujita, H., "Instantaneous Pressure Distribution Around a Sphere in Unsteady Flow," *Journal of Fluids Engineering*, Vol. 103, Dec. 1981, pp. 497–502.

[9]Loehrke, R. I., and Nagib, H. M., "Experiments on Management of Free-Stream Turbulence," AGARD-R-598, Sept. 1972.

[10]Zeiger, M. D., and Schaeffler, N. W., "Correcting Multi-Hole Probe Alignment Bias Errors Post Calibration," AIAA Paper 2001-0900, Jan. 2001.

[11]Johansen, E. S., "Development of a Fast-Response Multi-Hole Probe for Unsteady and Turbulent Flowfields," Ph.D. Dissertation, Aerospace Engineering Dept., Texas A&M Univ., College Station, TX, Dec. 2001.

R. Lucht
Associate Editor